Advances in Geosciences
Vol. 10: Atmospheric Science (2007)
Eds. J. H. Oh and G. P. Singh

SATELLITE-OBSERVED 3D MOISTURE STRUCTURE AND AIR–SEA INTERACTIONS DURING SUMMER MONSOON ONSET IN THE SOUTH CHINA SEA

YONGSHENG ZHANG
International Pacific Research Center, SOEST,
University of Hawaii at Manoa, POST Bldg. 401,
1680 East-West Road, Honolulu, Hawaii 96822, USA

TIM LI
International Pacific Research Center and Department of Meteorology,
SOEST, University of Hawaii at Manoa, POST Bldg 401,
1680 East-West Road, Honolulu, Hawaii 96822, USA

In this chapter, water vapor and air temperature profiles observed by the Atmospheric Infrared Sounder (AIRS), sea surface temperature (SST) and rain rate observed by TRMM Microwave Imager (TMI), and QuikSCAT surface wind for 2003–2006 are used to identify the 3D moisture structure and air–sea interaction processes during the onset of the South China Sea summer monsoon (SCSSM). Our analyses document an enhanced moisture accumulation in the atmospheric boundary layer co-existing with the surface easterlies preceding to the monsoon convection. Further analysis points out that, compared to the warming of SST, the boundary layer convergence plays a more important role in producing a warm and wet atmospheric boundary layer ahead of the monsoon convection, which contributes greatly to the development and maintenance of the northward propagation of the monsoon convection.

1. Introduction

As a semi-enclosed tropical sea surrounded by the Southeast–East Asian landmass, the South China Sea (SCS) plays an important role in modulation of climate anomalies in Asia. In middle May, accompanied by a switch of the prevailing zonal wind from easterly to westerly, the onset of the SCS summer monsoon (SCSSM) is characterized by an abrupt increase of precipitation and an associated tropical convergence zone northward propagating from the equator to northern SCS. The rainfall belt continues to move northward and controls the central China and South of Japan in late May and early

June.[1–3] On an interannual time-scale, the year-to-year variability of the SCSSM onset date and intensity in May has a strong projection onto the summer rainfall anomalous pattern in the East China and West Pacific Ocean, foreshadowing the development of the full-scale Asian summer monsoon during the subsequent months.[2,4–8] These scientific issues have called for a multi-national atmospheric and oceanographic observational and research plan, the SCS Monsoon Experiment (SCSMEX), which was aimed to a better understanding of the onset, maintenance, and variability of the SCSSM (for a overview, see Ref. 7).

In the past decades, efforts have been made to explore various aspects of the SCSSM and led to significant progress. However, some open issues still remain. For example, what is the driving mechanism of the SCSSM onset? While many studies focused on the large-scale environmental condition favorable for the SCSSM onset, the role of the local air–sea interaction and the three-dimensional water vapor profile has rarely been addressed, partially due to shortage of reliable observations in an appropriate time–space resolution. Using ship observations, Chu and Chang[9] identified the development of a warm-core eddy in the central SCS immediately before onset of the SCSSM attributing to the radiative warming and the downwelling driven by the surface anti-cyclonic flows, which helps lowering atmospheric surface pressure. However, their data analysis is limited to 1966 only. The air–sea heat exchanges during different stages of the SCSSM onset have also been explored by using the station observations in the SCS.[10–12] Though considerable air–sea flux exchanges were identified during the monsoon onset, the direction of the heat transportation varies from one study to another, partially because of the difference of the observation location and time.[12] So far there is no conclusive result on how the air–sea interaction and water vapor profile may affect the *in situ* thermodynamic condition which leads to the onset and northward propagation of the SCSSM.

The recently available satellite observations of the sea surface temperature (SST), precipitation, humidity, air temperature, and surface wind provide accurate and high-resolution coverage in the ocean regions where the conventional observation is rare. This provides an unprecedented opportunity to investigate the complicated physical processes relevant to the SCSSM onset. Among satellite sensors, the Atmospheric Infrared Sounder (AIRS) is a facility instrument aboard the NASA's Earth Observing System (EOS) polar-orbiting platform and is the most advanced moisture and air temperature sounding system. It constitutes an innovative atmospheric sounding group of visible, infrared, and microwave sensors

for measuring atmospheric water and temperature profiles with a twice-daily, 1–2 km vertical, and 45 km horizontal resolutions. The accuracy of the humidity and air temperature profiles derived from AIRS have been recognized as improving forecasts from meteorological prediction models.[a] The advantages of using the AIRS in describing the air temperature and moisture structures of the tropical Madden–Julian oscillation (MJO) have been demonstrated by a couple of studies.[13] (Yang *et al.*, 2006). The instruments carried by the Tropical Rainfall Measuring Mission (TRMM) satellites provide useful information of the tropical rain rate and SST. Also, NASA's Quick Scatterometer (QuikSCAT) offers the information of the surface wind.

In general, the goal of this chapter is to reveal the role of *in situ* hydrological cycle in driving the northward movement of the tropical convection during the SCSSM onset by analyzing the three-dimensional water vapor and the underlying air–sea interaction using the aforementioned satellite observations during 2003–2006.

2. Datasets

The level-3 AIRS data used in this study include the atmospheric moisture and temperature profiles at 12 levels from 1000 to 100 hPa with a spatially 1.0 degree longitude–latitude and a temporally twice-daily resolutions since 1 August 2002. Detail description of this dataset can be obtained at: http://disc.sci.gsfc.nasa.gov/AIRS. In this chapter, 10-day mean data are constructed from the original twice-daily data. We also used the 3-day running mean rain rate and SST observed by the TRMM Microwave Imager (TMI) and surface wind observed by the QuikSCAT. Both TMI rain rate, SST, and QuikSCAT wind have a resolution of 0.25×0.25 longitude/latitude and the information is provided at: http://www.ssmi.com. Other data used in this study include the daily reanalysis of the National Centers for Environmental Prediction (NCEP) and the National Center for Atmospheric Research (NCAR), and the global surface and upper air analyses at the European Centre for Medium-Range Weather Forecasts (ECMWF). The later is a 2.5×2.5 degree grid output from the ECMWF operational model provided through NCAR.

[a]NOAA administrator Lautenbacher has reported that "the AIRS instrument has provided the most significant increase in forecast improvement in this time range of any other single instrument." (http://daac.gsfc.nasa.gov/AIRS/).

3. Results

Previous studies have documented the weakness of the humidity in the reanalyses, particularly, at the lower troposphere. Zhang[14] compared the monthly humidity from the NCEP/NCAR and ECMWF 40-year reanalyses with the station observations in the East China in 1990s, and he found that the humidity in both the NCEP/NCAR and ECMWF 40-year reanalyses in the lower troposphere is much larger than that from the station observation, concurrent with a cold bias in the air temperature. Tian *et al.*[15] identified that the lower-troposphere moisture and temperature structure related to MJO is much less well defined in NCEP than in AIRS in the Pacific and Indian Oceans. In Fig. 1, we compare the 10-day mean humidity at 1000 hPa in May for 2003–2006 from AIRS observations with the NCEP/NCAR reanalysis. Overall, the magnitude in NCEP/NCAR reanalysis is larger than those of AIRS observations. In the SCS region, the moisture maximum in the AIRS observation locates in the ocean but in the NCEP/NCAR

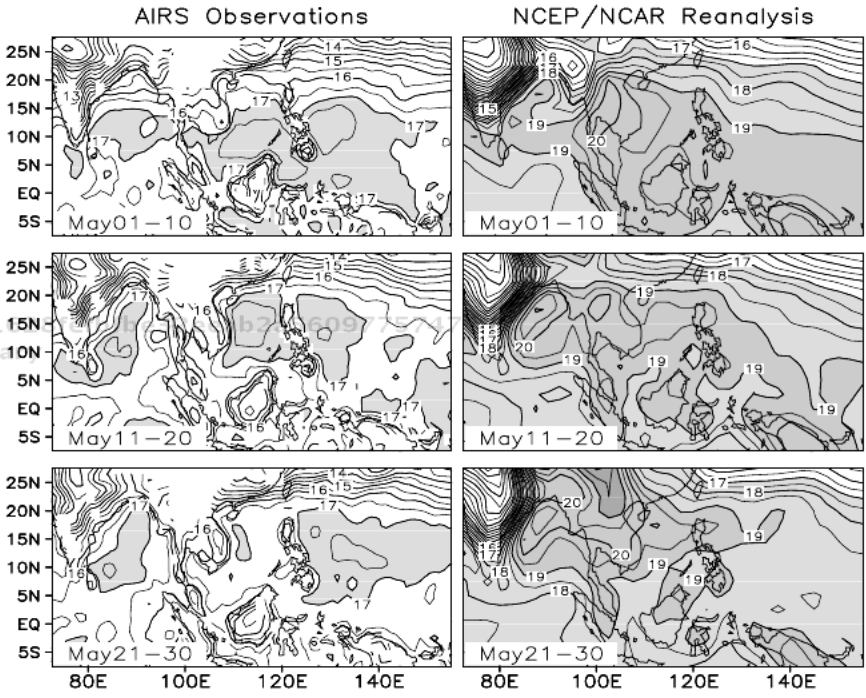

Fig. 1. 10-day mean specific humidity from AIRS observations (left panels) and from the NCEP/NCAR reanalysis (right panels) at 1000 hPa for 2003–2006 in unit of g/kg. Shaded areas denote the values lager than 17 g/kg for AIRS and 19 g/kg for NCEP/NCAR data.

reanalysis it mainly appears in the land region. In the northwestern Pacific region to east of Philippines, the AIRS observations show an independent maximum, but this does not occur in the NCEP/NCAR reanalysis. The results from AIRS observations also show a remarkable sub-seasonal change with decrease of the humidity from early to late May, consistent with a low-level moisture loss associated with a development of the strong convection activities in the SCS. However, this feature does not appear in the NCEP/NCAR reanalysis.

The 3D structure and evolution characteristics of the water vapor during the SCSSM onset have not been well documented. Figure 2 depicts the vertical distributions of the humidity, the QuiSCAT surface wind, and TMI precipitation averaged between 105°E–120°E in early, middle, and late May in 2003, 2004, and 2005, respectively. We did not discuss the case of 2006 simply because the onset of SCSSM in 2006 is strongly controlled by the circulation associated with Typhoon CHANCHU in middle May.

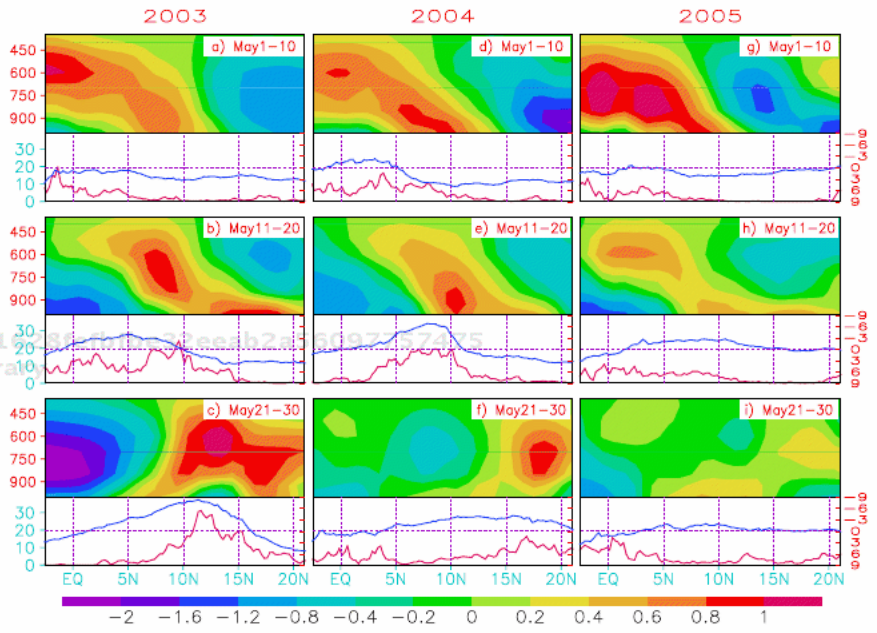

Fig. 2. The vertical-latitude distributions of the 10-day mean AIRS humidity at 1000 hPa (shading, scales are shown in the bar in unit of g/kg), QuiSCAT surface zonal wind (blue line, Y-coordinate scales are marked in right side in unit of m/s) and TMI rain rate (red line, Y-coordinate scales are marked in left side in unit of mm/day) averaged between 105°E and 120°E. For the humidity, Y-coordinate shows the pressure level (hPa) and the domain average over 105°E–120°E and eq.-20°N is removed at each pressure level.

Generally, the onset of the SCSSM is accompanied by a well-defined vertical southward-tilting moisture structure in the southern and central SCS in early and middle May (Fig. 2). In 2003, the enhanced convective activities occur in middle May in the central SCS around 12°N–15°N (Fig. 2(b)), signaling the onset of the SCSSM. Then, the rainfall maximum moves northward in late May (Fig. 2(c)). In 2004, strong rainfall starts in the southern SCS in early May (Fig. 2(d)), and then the rainfall maximum moves northward in middle and later May (Figs. 2(f) and (g)). In 2005, the convective activities in May are much weaker compared to those in 2003 and 2004, but the northward propagation of the convective activities from the southern to northern SCS is still seen clearly.

The most important feature depicted in Fig. 2 is that the rainfall maximum is preceded by water vapor maximum in the atmospheric boundary layer (ABL, around 900–1000 hPa) and is followed by a dry phase. The former is overlapping with easterlies, and latter with westerlies. In 2003, the vapor maximum in the low-to-middle troposphere (850–500 hPa) is clearly concurrent with the rainfall maximum (Figs. 2(a) and (b)). But near the surface the water vapor maximum occurs in the front of the rainfall maximum and is confined in the easterly prevailing region. The feature can also be clearly identified in 2004 and 2005 (Figs. 2(d), (e), (g), and (h)). This indicates that the enhanced moisture accumulation in the ABL in front of the monsoon convection plays an active role in leading the northward movement of the convection.

In order to identify what causes an enhanced moisture accumulation in ABL in front of the monsoon convection, we plot the south–north distributions of the AIRS humidity at 1000 hPa, TMI SST, ECMWF analyzed latent heat flux, QuikSCAT wind divergence, and TMI rain rate along 105°E–120°E during early, middle, and late May. Figure 3 presents the result in 2003 and the following features are noteworthy:

(1) The 1000 hPa humidity experiences a sharply decrease from early to middle May (Fig. 3(a), thin solid and dashed lines), when strong monsoon rainfall occurs in the southern SCS (south of 10°N). But it recovers in late May (Fig. 3(a) thick solid line), as the monsoon rainfall moves into the northern SCS with maximum in the region of 10°N–15°N. In the northern SCS (north to 10°N), the decrease of humidity in ABL is coincident with a maximum rainfall moving from the southern SCS (Figs. 3(a) and (e), thick solid line).
(2) A decrease of SST occurs from early to late May in the southern SCS is concurrent with a rapid increase of SST in the northern SCS

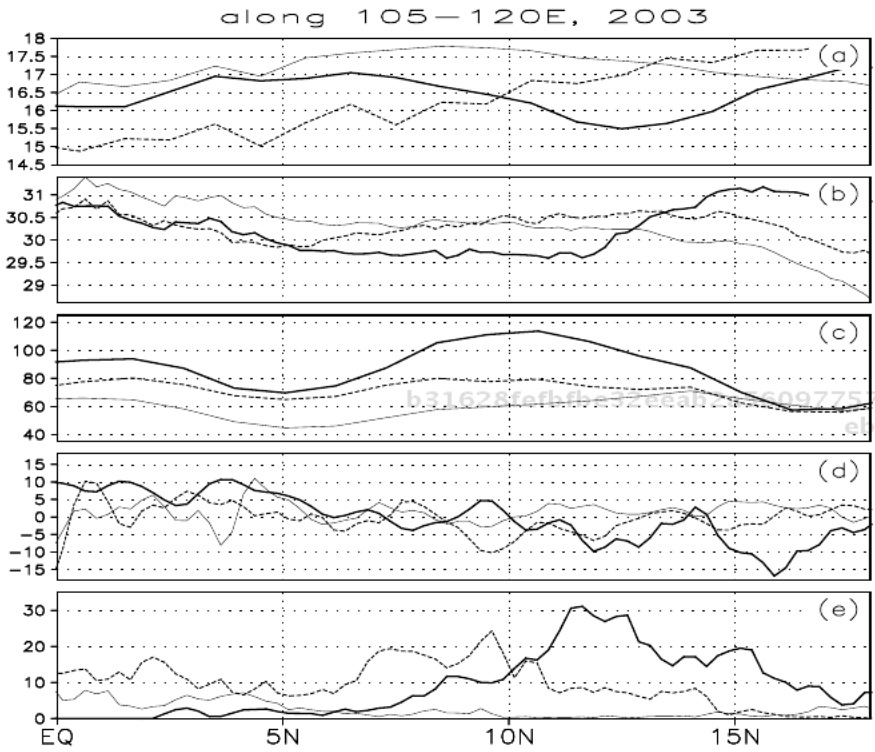

Fig. 3. The 10-day average of south–north distributions of (a) the AIRS humidity at 1000 hPa (g/kg), (b) SST (°C), (c) latent heat flux from the ocean to the atmosphere (w/m^2), (d) divergence calculated from the QuikSCAT surface wind (10^{-6} s), and (e) TMI rain rate (mm/day) along 105°E–120°E during May 1–10 (solid thin line), May 11–20 (dashed line), and May 21–30 (thick solid line) in 2003.

(Fig. 3(b)). This implies that the ocean and atmospheric physical processes associated with development of the strong monsoon rainfall tend to decrease the underlying SST, but to warm the SST in front of the rainfall maximum.

(3) The decrease of the moisture in ABL in the southern SCS in middle May (Fig. 3(a), dashed line) and in the northern SCS in late May (Fig. 3(c), solid thick line) are concurrent with an increase of the latent heat flux (Fig. 3(c)) relevant to a burst of westerly in these two regions (Figs. 2(b) and (c), blue lines), indicating that the moisture change at ABL is not attributed to the surface evaporation.

(4) While a strong convection maximum co-locates with a strong convergence near the surface, convergence also occurs in front of the

rainfall maximum, tending to overlap the region of enhanced moisture (Fig. 3(d)).

Figure 4 shows the same plot for 2004. The strong monsoon rainfall first appears in the southern SCS in early May and then moves to northern SCS. In middle May, the development of strong monsoon rainfall in the central SCS (Fig. 4(e), dashed line) is concurrent with a reduced humidity (Fig. 4(a), dashed line) and SST (Fig. 4(b)), but an increased latent heat flux transporting from the ocean to the atmosphere in the southern SCS (Fig. 4(c)). The convergence mainly locates to the front of the rainfall maximum (Fig. 4(d)). Similar to 2003, a decrease of SST in the region south to 10°N is accompanying with an increase in the northern part. In late May, a pronounced decrease of SST in the central–northern SCS coincides with

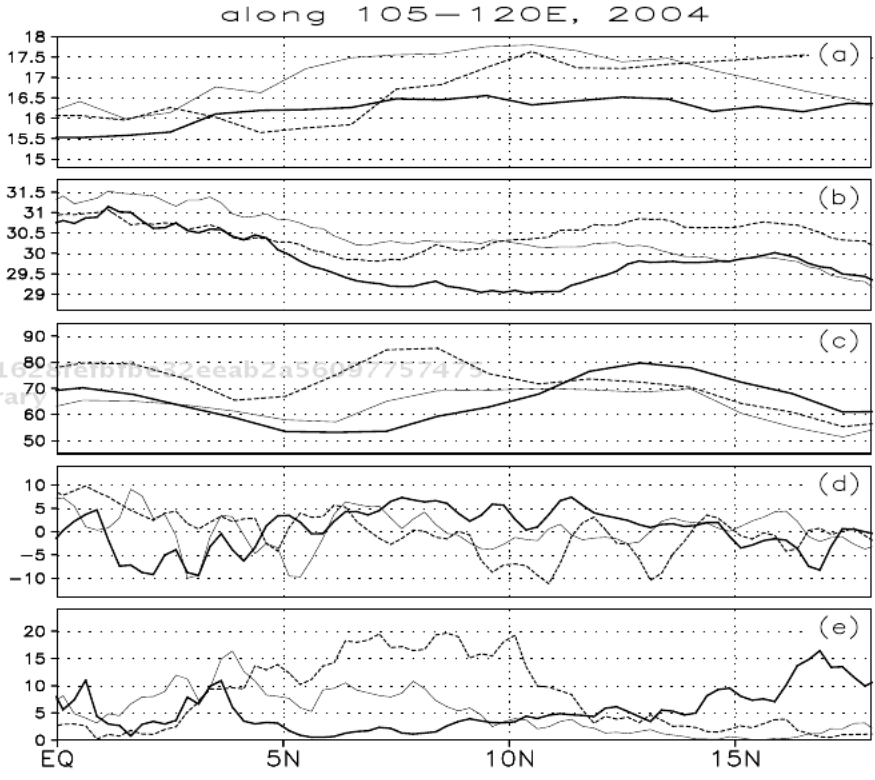

Fig. 4. Same as Fig. 3, but for the year of 2004.

an increase of the latent heat flux in the northern SCS, just behind the rainfall maximum.

It is interesting to note that, in Figs. 3 and 4, the maximum of evaporation reflected by the latent heating flux is not coincident with the enhanced moisture accumulation in front of the intense convection in early and middle May. In both 2003 and 2004, while a remarkable increase of SST and moisture occurs in the northern SCS in middle May (Figs. 5(a) and (b)), the latent heat flux has a minimum change (Fig. 5(c)). The maximum increase in latent heat flux between 5°N and 10°N is primarily due to the increase in the surface wind speed (Fig. 5(d)), and it coexists with a SST cooling (Fig. 5(b)) and a sharp decrease of the humidity. When the latent heating flux maximum moves into the northern SCS in late May in 2003

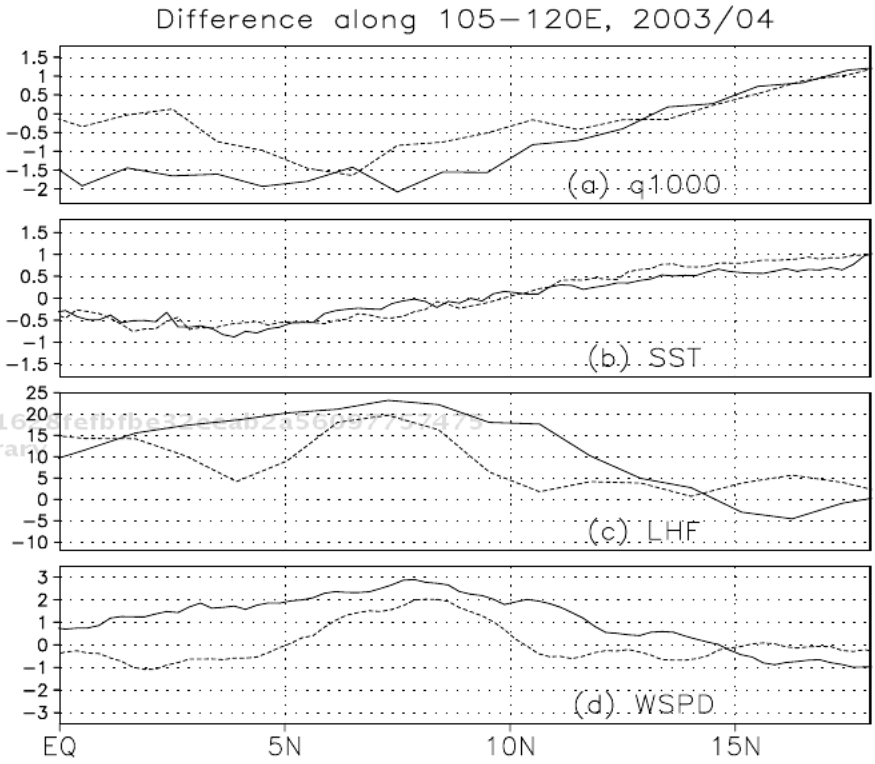

Fig. 5. The difference of 10-day average between May 11–20 and May 1–10 in 2003 (solid lines) and 2004 (dashed lines) of (a) the AIRS humidity at 1000 hPa (g/kg), (b) SST (°C), (c) latent heat flux from the ocean to the atmosphere (w/m^2), and (d) wind speed (m/s) along 105°E–120°E.

and 2004, the humidity near the surface in the northern SCS decreases. The results indicate that, while a SST warming is concurrent with a moistening ABL in front of the monsoon convection, this warming does not directly contribute to the moistening. Above features can also be found in the year of 2005 though, compared to 2003 and 2004, the strength of the monsoon rainfall and associated wind are not as strong as those in 2003 and 2004.

As shown in Figs. 3(d) and 4(d), lower-level convergence not only coincides with the convection but also appears in front of the rainfall maximum and is co-located with the region of maximum boundary-layer humidity. This suggests that the convergence in the ABL is one of dominant

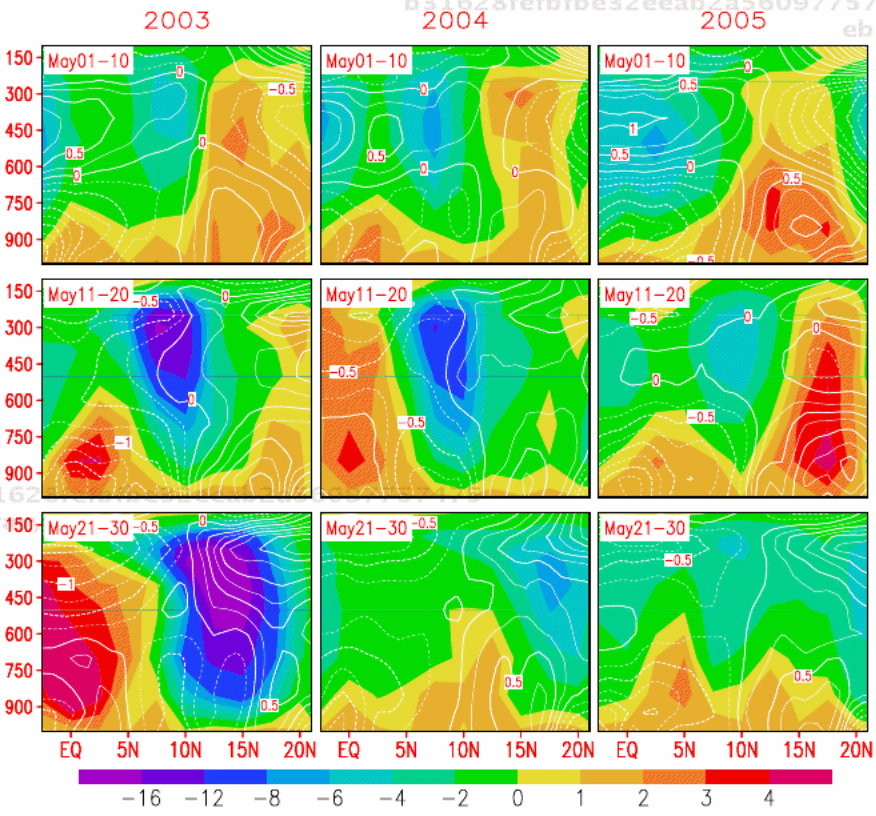

Fig. 6. The latitude-pressure cross-sections of the ECMWF vertical velocity (Omega, shading and scales are shown by the bar in unit of 10^{-2} Pa/s) and AIRS air temperature (contours, with an interval of 0.25°C) averaged along 105°E–120°E. A domain average over 105°E–102°E and eq-20°N is removed from the air temperature at each pressure level.

processes responsible for an enhanced vapor accumulation in front of the convection.

Figure 6 presents the latitude-pressure cross-sections of the vertical velocity (Omega) from ECMWF analysis and the air temperature observed by AIRS averaged along 105°E–120°E. A domain average over 105°E–102°E and eq.-20°N is removed from the air temperature at each level in order to emphasize its north–south gradient. It can be seen that, during monsoon onset in 2003, 2004, and 2005, the northward movement of the advanced convection in Fig. 2 (red lines) is associated with strongly ascending motion between 600 and 200 hPa (Fig. 6, shading). In the pre-onset phase during early May, a weak descending branch is found in front of the convection maximum. During the mature onset phase (middle May), the descending motion weakens and is confined below 700 hPa in 2003 and 2004. The weak descending motion in front of the monsoon convection helps to preserve the converged moisture near the surface. The air temperature profile observed from AIRS satellite show that a relatively warm center lies in front of the rainfall maximum while a cold one overlapping the rainfall maximum. Therefore, the monsoon rainfall maximum is overlapped and followed by a dry-cold ABL and preceded by a warm–wet one. This provides a favorable condition for the northward migration of the convection from southern to northern SCS.

4. Summary and Discussion

Using the high-resolution moisture and air temperature data observed by the AIRS, tropical rain rate and SST by TRIMM and QuiSCAT surface wind field for 2003–2005, we investigate the 3D moisture structure and air temperature, and air–sea interactions involved in northward movement of the strong convective activities during the summer monsoon onset in the SCS. Our special attention is paid to reveal how the regional circulation related to the monsoon onset in the SCS contributes to the *in situ* air–sea interactions and moisture distributions which, in turn, provide a favorable condition for development and maintenance of the tropical convective activities, and the northward propagation of the monsoon rainfall. The results show that the SCSSM onset in 2003, 2004, and 2005 shows some common features. Most interestingly, we find that the intense convective activities are preceded by an enhanced moisture accumulation and warm air temperature near the surface and followed by a dry and cold ABL. The vertical profile shows a southward-tilting structure. The

wet ABL in front of the monsoon rainfall maximum is co-located with easterly wind, and the maximum of the latent heat flux transporting from the ocean to the atmosphere concurs with the burst of the westerly behind the convective maximum and tends to coexist with a SST cooling and a water vapor decrease near the surface. Therefore, despite the in-phase relation between the enhanced moisture accumulation and increased SST in front of the monsoon rainfall maximum, the SST warming and associated evaporation do not directly contribute to the humidity increase.

Our diagnosis also shows that the warm and wet ABL in front of the monsoon rainfall maximum tends to be concurrent with a near-surface convergence. Therefore, it is likely that the lower-level convergence is the major contributor for the moisture increase. In contrast to Fu *et al.*,[13] our study emphasizes the role of the regional convergence preceding the monsoon rainfall in determining the enhanced moisture accumulation. This result is in agreement with the observational and theoretical study by Jiang *et al.*,[16] who pointed out that the preceding distribution of the boundary-layer convergence is one of the mechanisms that contributes to a northward propagation of the intraseasonal convection.

A special feature of the current study is to reveal a more conclusive and systematical scenario on the regional feedback between the atmospheric moisture, air temperature, and SST response to the intense monsoonal convections with the aid of the fine-resolution satellite observations from AIRS, TMI, and QuikSCAT instruments. More detail linkage needs to be further identified with the help of the ocean data and an accurate estimation of the surface heat fluxes. In these feedbacks, we observe that the warm and wet ABL provides more unstable condition preceding the convective maximum, and strong temperature gradients associated with warming (cooling) in front of (behind) the convection, in turn, make a great contribution to the northward propagation of the monsoon convective activities.

Acknowledgments

TL was supported by ONR grants N000140710145 and N000140210532 and NRL subcontract N00173-06-1-G031. The International Pacific Research Center is partially sponsored by the Japan Agency for Marine-Earth Science and Technology (JAMSTEC).

References

1. S. Y. Tao and L. X. Chen, *Monsoon Meteorology* (Oxford University Press, 1987), p. 60.
2. K. M. Lau and S. Yang, *Adv. Atmos. Sci.* **14** (1997) 141.
3. B. Wang and L. Ho, *J. Clim.* **15** (2002) 386.
4. C. H. So and J. C. L. Chan, *J. Meteor. Soc. Jpn.* **75** (1997) 43.
5. B. Wang and R. Wu, *Adv. Atmos. Sci.* **14** (1997) 177.
6. C. Li and L. Zhang, *Chinese J. Atmos. Sci.* **23** (1999) 257.
7. Y. Ding, C. Li and Y. Liu, *Adv. Atmos. Sci.* **21** (2004) 343.
8. R. Huang, L. Gu, L. Zhou and S. Wu, *Adv. Atmos. Sci.* **23** (2006) 909.
9. P. C. Chu and C.-P. Chang, *Adv. Atmos. Sci.* **14** (1997) 195.
10. X. Bai, A. Wu and Y. Zhao, *Onset and Evolution of the South China Sea Monsoon and Its Interaction with the Ocean* (China Meteor. Press, 1999), p. 381.
11. J. Yan *et al.*, *Acta Ocea. Sin.* **22** (2004) 369.
12. D. Wu *et al.*, *Chinese Sci. Bull.* **51** (2006) 2413.
13. X. Fu, B. Wang and L. Tao, *Geophys. Res. Lett.* **33** (2006) L03705.
14. Y. Zhang, *Biases of NCEP/NCAR and ECMWF 40-Year Re-Analyses in East Asia*, IAMAS 2005 Scientific Assembly, August 2–11, 2005, Beijing, China.
15. B. Tian *et al.*, *J. Atmos. Sci.* **63** (2006) 2462.
16. X. Jiang, T. Li and B. Wang, *J. Clim.* **17** (2004) 1022.